Electronic Supplementary Information (ESI)

Heteroanion-introduction-driven birefringence enhancement in oxychalcogenide $Ba_3M^{II}Ge_3O_2S_8$ (M^{II} = Mn, Cd)

Sheng-Hua Zhou,‡[a,b,c] Mao-Yin Ran,‡[a,b,c] Wen-Bo Wei,[a,b,c] A-Yang Wang,[a,b,d] Xin-Tao Wu,[a,b] Hua Lin,*[a,b] and Qi-Long Zhu*[a,b]

[a]*State Key Laboratory of Structural Chemistry, Fujian Institute of Research on the Structure of Matter, Chinese Academy of Sciences, Fuzhou 350002, China*

[b]*Fujian Science & Technology Innovation Laboratory for Optoelectronic Information of China, Fuzhou, Fujian 350108, China*

[c]*University of Chinese Academy of Sciences, Beijing 100049, China*

[d]*College of Chemistry, Fuzhou University, Fujian 350002, China*

‡S. H. Zhou and M. Y. Ran contributed equally to this work.

*E-mail: linhua@fjirsm.ac.cn and qlzhu@fjirsm.ac.cn.

Table of Contents

4 References

Electronic Supplementary Information (ESI)

1 Experimental Section

1.1 Materials and Instruments

All reagents used in the present experiments were purchased from commercial sources and directly used without further purification. All weighing processes were completed in an anhydrous and oxygen-free glove box. The semi-quantitative energy dispersive X-ray (EDX, Oxford INCA) spectra were measured with a field emission scanning electron microscope (FESEM, JSM6700F). Powder X-ray diffraction (XRD) analysis was carried out in a Rigaku Mini-Flex II powder diffractometer (Cu-K_α, λ = 1.5418 Å). UV-vis-NIR absorption measurement was performed in the region of 200−2500 nm at room temperature using an UV-vis-NIR spectrometer (Perkin-Elmer Lambda 950). The reflectance spectrum of the $BaSO_4$ powder was collected as the baseline and the diffuse reflectance data were converted to absorbance internally by the instrument by use of the Kubelka-Munk function.[1] The thermal stability analyses were measured on a NETZSCH STA 449C simultaneous analyser.

1.2 Synthesis

The crystals of $Ba_3M^{II}Ge_3O_2S_8$ (M^{II} = Mn, Cd) were synthesized with a high yield of 70% (based on M^{II}) through a high-temperature solid-state reaction. The raw materials, including 1 mmol BaO (0.153 g, Macklin, 99.95%), 0.33 mmol MnS (0.029 g, Aladdin, 98%), 0.33 mmol CdS (0.048 g, Aladdin, 99.999%) and 1 mmol Ge (0.073 g, Macklin, 99.999%) and 2 mmol S (0.064 g, Aladdin, 99.99%), were ground to a consistent mixture without further purification. The mixture was then heated from room temperature to 673 K. After holding at 673 K for 20 hours, the temperature was raised to 1223 K in 30 hours. The furnace was kept at the highest temperature for 100 hours and then gradually cooled down to 523 K within 150 hours. Finally, the crystals

were brought back to room temperature naturally without any additional heating. After washing the crystals with deionized water and ethanol, the $Ba_3M^{II}Ge_3O_2S_8$ (M^{II} = Mn, Cd) were obtained. These crystals remained stable in both air and moisture. To determine the crystal structure, a selection of high-quality single crystals of $Ba_3M^{II}Ge_3O_2S_8$ (M^{II} = Mn, Cd) were made.

1.3 Birefringence Measurements

The birefringence (Δn) was characterized by using the polarizing microscope (ZEISS Axio Scope, A1) equipped with Berek compensator. The wavelength of the light source was 546 nm. The formula for calculating the Δn is $R = | N_e – N_o | \times T = \Delta n \times T$. Here, R represents the optical path difference and T denotes the thickness of the crystal.

1.4 Single-Crystal Structure determination

Taking some high-quality crystals of $Ba_3M^{II}Ge_3O_2S_8$ (M^{II} = Mn, Cd) with suitable sizes were selected for single-crystal X-ray diffraction (XRD) analysis. The single-crystal diffraction data collections were collected on a Saturn 724 install with graphite-monochromated Mo-K_α radiation (λ = 0.71073 Å) at room temperature.The absorption correction was performed by the multi-scan method.[2] Using direct methods and maken further refinement by full-matrix least-square fitting on F^2 based on *SHELX−2014* software, the precise struture was determined sussessfully.[3] Crystal data and structure refinement parameters were given in Table 1. The final refined atomic positions and isotropic thermal parameters are listed in Table S1. Interatomic distances (Å) and bond angles (deg) are displayed in Table S2 and Table S3. CIFs of

$Ba_3MnGe_3S_8O_2$ and $Ba_3CdGe_3S_8O_2$ have been submitted with CCDC numbers 2234468 and 2234469.

2 Computational Details

The DFT calculations have been performed using the *Vienna ab initio simulation package* (VASP)[4–6] with the Perdew-Burke-Ernzerhof (PBE)[7] exchange correlation functional. The projected augmented wave (PAW)[8] potentials with the valence states 4d, 5p and 6s for Ba, 4s, 4p and 3d for Mn, 5s, 5p and 4d for Cd, 4s and 4p for Ge, 3s and 3p for S, 2s and 2p for O respectively, have been used. A Γ-centered 7×7×9 Monkhorst-Pack grid for the Brillouin zone sampling[9] and a cutoff energy of 800 eV for the plane wave expansion were found to get convergent lattice parameters.

3 Figures and Tables

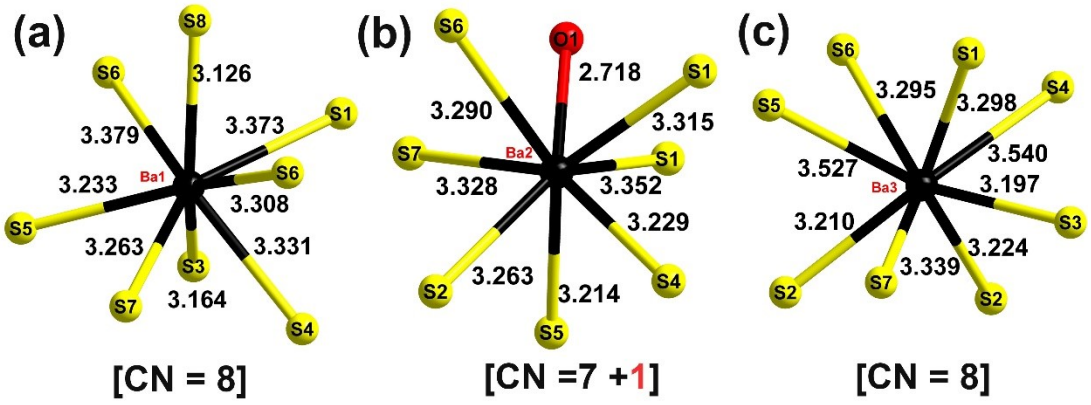

Figure S1. Coordination environments and bond distances of the Ba atoms in $Ba_3CdGe_3O_2S_8$.

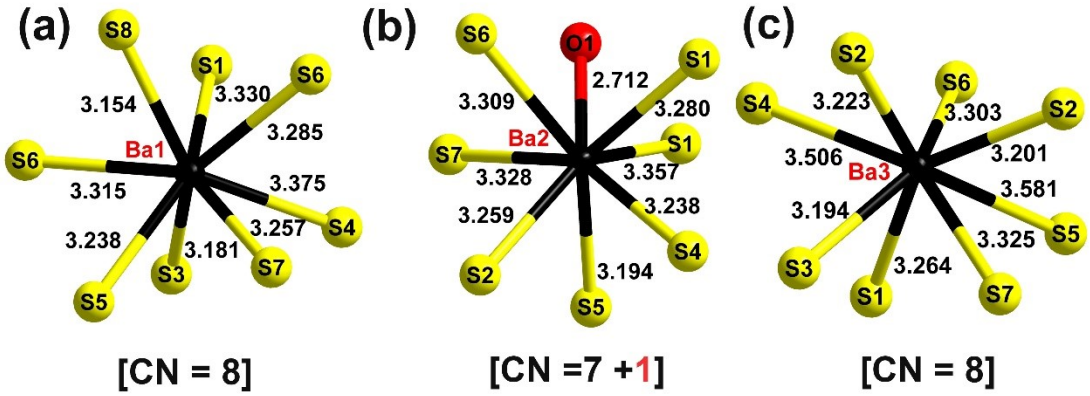

Figure S2. Coordination environments and bond distances of the Ba atoms in $Ba_3MnGe_3O_2S_8$.

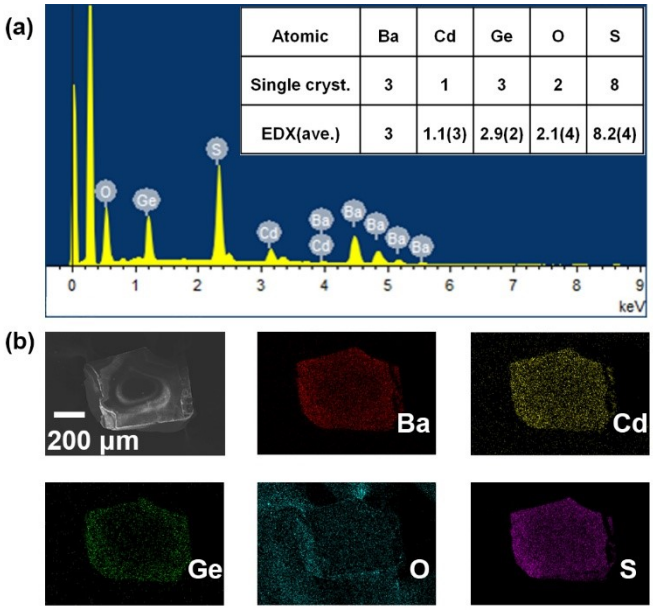

Figure S3. The characterizations of $Ba_3CdGe_3O_2S_8$: (a) EDX results and (b) SEM image and corresponding elemental mapping analysis.

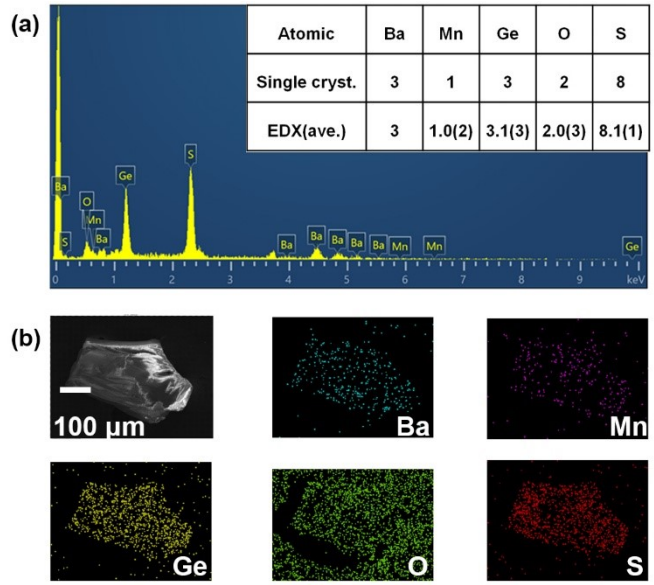

Figure S4. The characterizations of $Ba_3MnGe_3O_2S_8$: (a) EDX results and (b) SEM image and corresponding elemental mapping analysis.

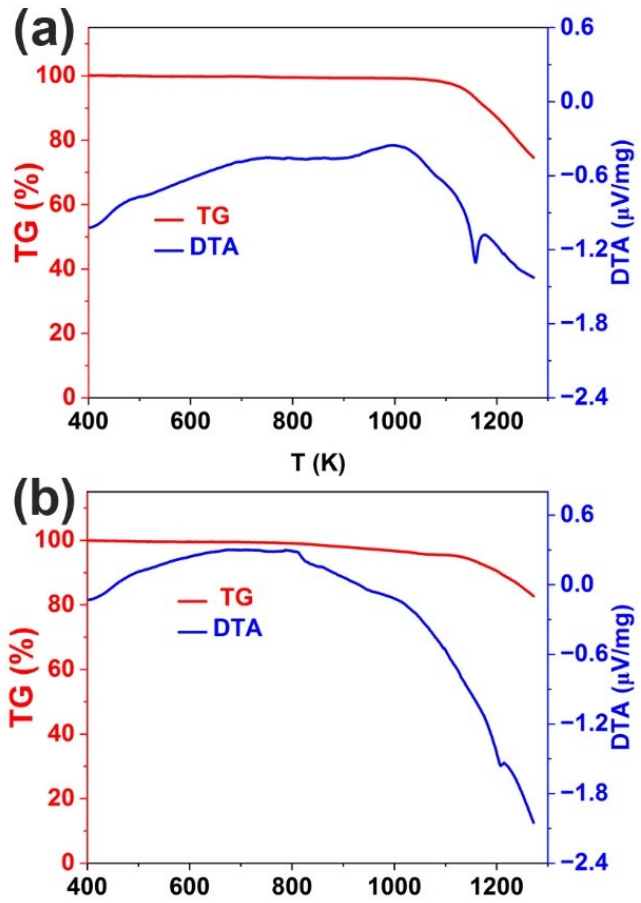

Figure S5. The TG-DTA curves of (a) $Ba_3CdGe_3O_2S_8$ and (b) $Ba_3MnGe_3O_2S_8$.

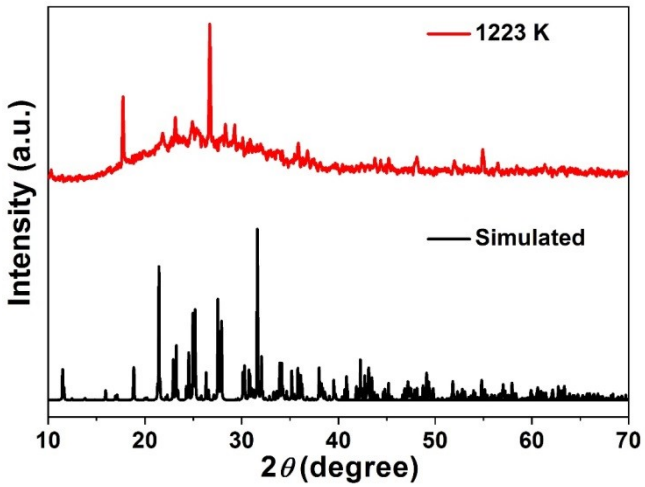

Figure S6. Experimental and simulated powder XRD patterns for as-synthesized $Ba_3CdGe_3O_2S_8$ after calcining at 1223 K.

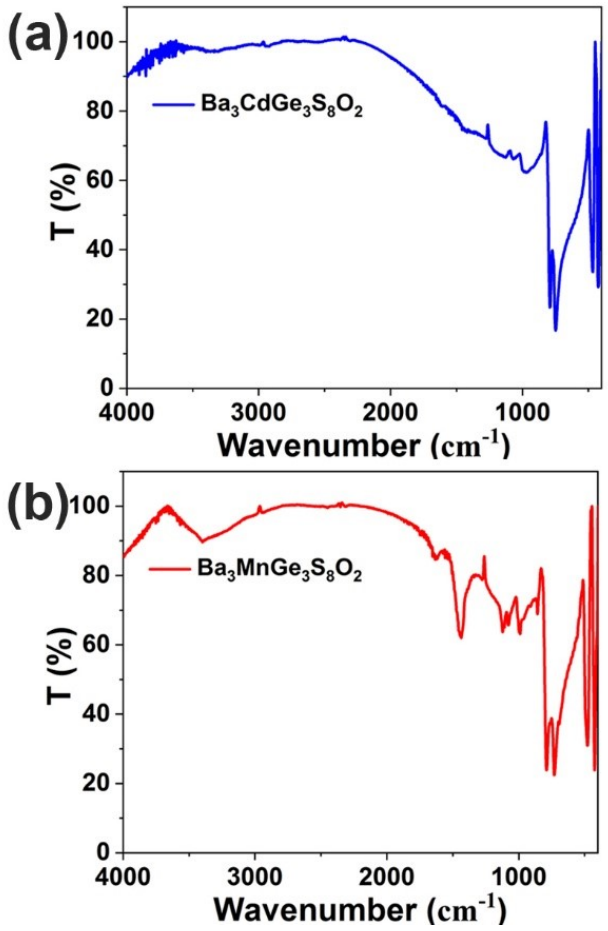

Figure S7. The infrared spectrum of (a) $Ba_3CdGe_3O_2S_8$ and (b) $Ba_3MnGe_3O_2S_8$.

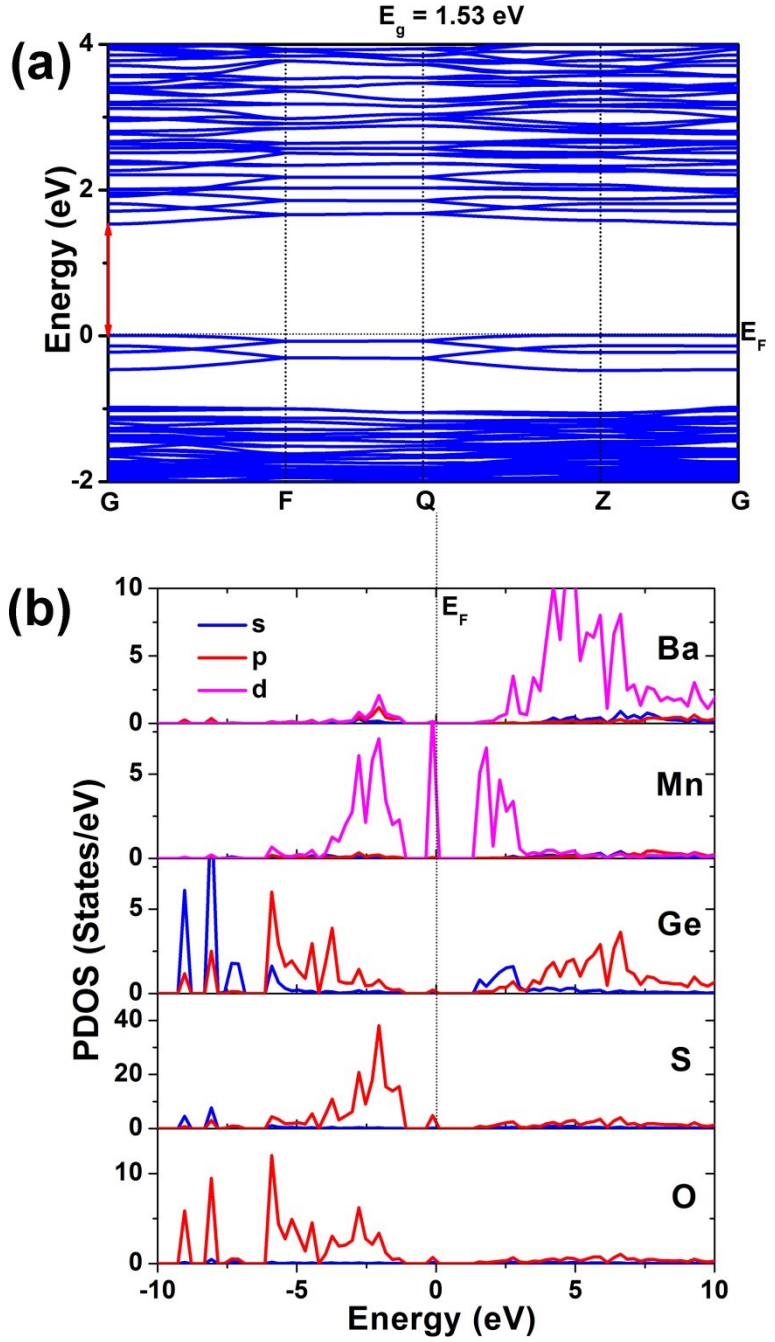

Figure S8. Theoretical calculations of $Ba_3MnGe_3O_2S_8$: (a) calculated band structure and (b) PDOS.

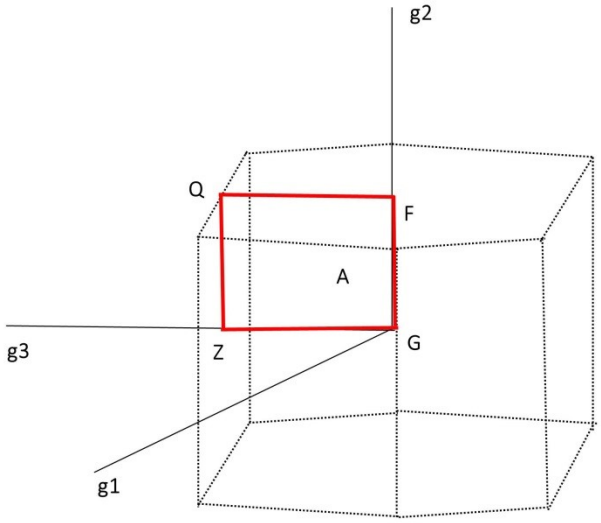

Figure S9. The first Brillouin zone with high symmetry points of $Ba_3M^{II}Ge_3O_2S_8$ (M^{II} = Mn, Cd).

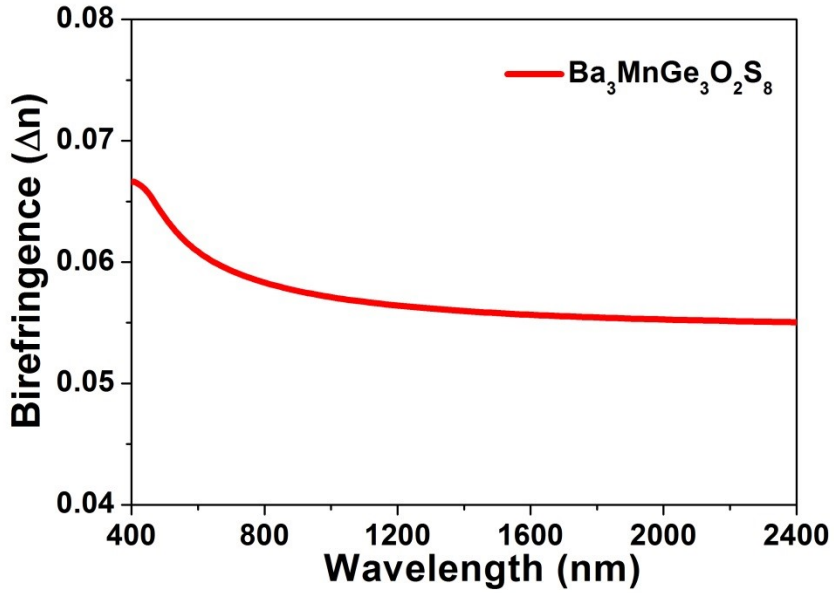

Figure S10. Calculated birefringence of $Ba_3MnGe_3O_2S_8$.

Electronic Supplementary Information (ESI)

Table S1. Atomic coordinates and equivalent isotropic displacement parameters of $Ba_3M^{II}Ge_3S_8O_2$ (M^{II} = Mn, Cd).

atom	wyckff	x	y	z	U_{eq}(Å)^2	*BVS*
			$Ba_3CdGe_3O_2S_8$			
Ba1	4*e*	0.61797(5)	0.46476(4)	0.24267(3)	0.01342(14)	2.11
Ba2	4*e*	0.59849(5)	0.19216(4)	0.46103(3)	0.01309(14)	2.06
Ba3	4*e*	0.61754(5)	0.18371(4)	0.03346(3)	0.01604(14)	1.86
Cd	4*e*	0.33572(7)	0.77405(5)	0.26018(4)	0.01996(17)	1.97
Ge1	4*e*	0.21583(9)	0.04279(6)	0.41639(5)	0.00976(18)	4.11
Ge2	4*e*	0.03927(8)	0.56983(6)	0.24598(5)	0.00913(18)	4.19
Ge3	4*e*	0.31322(9)	0.54954(7)	0.39890(5)	0.01086(18)	4.04
S1	4*e*	0.7937(2)	0.42658(16)	0.05066(12)	0.0139(4)	1.96
S2	4*e*	0.7955(2)	0.42286(16)	0.47637(13)	0.0151(4)	1.99
S3	4*e*	0.4657(2)	0.65431(16)	0.12659(12)	0.0149(4)	2.07
S4	4*e*	0.3383(2)	0.36702(16)	0.11560(12)	0.0127(4)	2.02
S5	4*e*	0.5126(2)	0.65533(16)	0.37908(12)	0.0141(4)	2.08
S6	4*e*	0.6478(2)	0.18849(16)	0.24832(12)	0.0124(4)	2.03
S7	4*e*	0.3536(2)	0.37120(16)	0.37038(12)	0.0132(4)	1.98
S8	4*e*	0.9578(2)	0.40782(17)	0.28172(15)	0.0206(4)	2.2
O1	4*e*	0.3869(6)	0.0839(5)	0.3616(3)	0.0155(11)	2.06
O2	4*e*	0.1953(7)	0.6137(5)	0.3125(4)	0.0231(13)	1.95
			$Ba_3MnGe_3O_2S_8$			
Ba1	4*e*	0.62426(9)	0.46074(7)	0.24496(5)	0.0159(2)	2.12
Ba2	4*e*	0.59732(9)	0.19119(7)	0.46197(5)	0.0156(2)	2.09
Ba3	4*e*	0.61487(10)	0.18562(7)	0.03132(6)	0.0183(2)	1.89
Mn	4*e*	0.3334(3)	0.76541(19)	0.25962(14)	0.0205(5)	1.80
Ge1	4*e*	0.21263(16)	0.04063(11)	0.41546(9)	0.0127(3)	4.0
Ge2	4*e*	0.04136(15)	0.56594(11)	0.24544(9)	0.0110(3)	4.17
Ge3	4*e*	0.31445(16)	0.54838(12)	0.39803(9)	0.0132(3)	3.98
S1	4*e*	0.7898(4)	0.4275(3)	0.0513(2)	0.0158(7)	1.98
S2	4*e*	0.7937(4)	0.4239(3)	0.4760(2)	0.0173(7)	1.99
S3	4*e*	0.4664(4)	0.6533(3)	0.1306(2)	0.0189(7)	2.01
S4	4*e*	0.3367(4)	0.3636(3)	0.1185(2)	0.0144(7)	1.95
S5	4*e*	0.5120(4)	0.6572(3)	0.3772(2)	0.0168(7)	2.06
S6	4*e*	0.6481(4)	0.1835(3)	0.2473(2)	0.0152(7)	2.06
S7	4*e*	0.3516(4)	0.3683(3)	0.3682(2)	0.0165(7)	1.96
S8	4*e*	0.9678(4)	0.4007(3)	0.2793(3)	0.0251(8)	2.18
O1	4*e*	0.3855(11)	0.0832(9)	0.3629(6)	0.018(2)	2.07
O2	4*e*	0.1998(12)	0.6159(9)	0.3096(6)	0.022(2)	1.80

U_{eq} is defined as one third of the trace of the orthogonalized U_{ij} tensor.

Table S2. Selected bond lengths (Å) and angle (°) of $Ba_3CdGe_3O_2S_8$.

Cd–O2	2.422(6)	∠O2–Cd–S5	70.47(14)
Cd–S3	2.758(2)	∠S8–Cd–S5	95.05(7)
Cd–S4	2.700(2)	∠S4–Cd–S5	93.97(6)
Cd–S5	2.770(2)	∠S3–Cd–S5	89.13(6)
Cd–S7	2.834(2)	∠O2–Cd–S7	104.86(14)
Cd–S8	2.514(2)	∠S8–Cd–S7	89.03(7)
		∠S4–Cd–S7	89.55(6)
Ge1–O1	1.806(5)	∠S3–Cd–S7	86.40(6)
Ge1–S1	2.187(2)	∠S5–Cd–S7	173.36(6)
Ge1–S3	2.178(2)		
Ge1–S4	2.205(2)	∠O1–Ge1–S3	108.10(19)
		∠O1–Ge1–S1	97.88(18)
Ge2–O1	1.787(5)	∠S3–Ge1–S1	113.66(8)
Ge2–O2	1.779(5)	∠O1–Ge1–S4	109.60(18)
Ge2–S6	2.178(2)	∠S3–Ge1–S4	110.99(8)
Ge2–S8	2.137(2)	∠S1–Ge1–S4	115.57(8)
		∠O2–Ge2–O1	102.1(3)
Ge3–O2	1.838(6)	∠O2–Ge2–S8	112.4(2)
Ge3–S2	2.174(2)	∠O1–Ge2–S8	116.7(2)
Ge3–S5	2.191(2)	∠O2–Ge2–S6	111.5(2)
Ge3–S7	2.203(2)	∠O1–Ge2–S6	105.24(18)
		∠S8–Ge2–S6	108.63(8)
∠O2–Cd–S8	164.29(15)	∠O2–Ge3–S2	108.4(2)
∠O2–Cd–S4	78.04(16)	∠O2–Ge3–S5	96.2(2)
∠S8–Cd–S4	109.94(6)	∠S2–Ge3–S5	113.60(8)
∠O2–Cd–S3	93.22(16)	∠O2–Ge3–S7	110.6(2)
∠S8–Cd–S3	80.13(6)	∠S2–Ge3–S7	113.28(8)
∠S4–Cd–S3	169.10(6)	∠S5–Ge3–S7	113.36(8)

Table S3. Selected bond lengths (Å) and angle (°) of $Ba_3MnGe_3O_2S_8$.

Mn–O2	2.262(10)	∠O2–Mn–S5	73.1(3)
Mn–S3	2.655(4)	∠S8–Mn–S5	93.15(14)
Mn–S4	2.667(4)	∠S4–Mn–S5	94.18(12)
Mn–S5	2.698(4)	∠S3–Mn–S5	89.74(12)
Mn–S7	2.808(4)	∠O2–Mn–S7	105.7(3)
Mn–S8	2.452(4)	∠S8–Mn–S7	87.84(14)
		∠S4–Mn–S7	88.11(12)
Ge1–O1	1.802(9)	∠S3–Mn–S7	87.76(12)
Ge1–S1	2.206(4)	∠S5–Mn–S7	177.11(13)
Ge1–S3	2.199(4)		
Ge1–S4	2.205(2)	∠O1–Ge1–S3	107.5(3)
		∠O1–Ge1–S1	96.6(3)
Ge2–O1	1.791(9)	∠S3–Ge1–S1	114.49(14)
Ge2–O2	1.799(10)	∠O1–Ge1–S4	109.1(3)
Ge2–S6	2.179(4)	∠S3–Ge1–S4	110.99(8)
Ge2–S8	2.125(4)	∠S1–Ge1–S4	111.42(14)
		∠O2–Ge2–O1	100.3(5)
Ge3–O2	1.858(10)	∠O2–Ge2–S8	114.1(3)
Ge3–S2	2.178(4)	∠O1–Ge2–S8	116.3(4)
Ge3–S5	2.193(4)	∠O2–Ge2–S6	110.9(4)
Ge3–S7	2.203(4)	∠O1–Ge2–S6	105.0(3)
		∠S8–Ge2–S6	109.74(15)
∠O2–Mn–S8	165.6(3)	∠O2–Ge3–S2	109.5(4)
∠O2–Mn–S3	95.5(3)	∠O2–Ge3–S5	94.1(3)
∠S8–Mn–S3	79.84(13)	∠S2–Ge3–S5	113.30(14)
∠O2–Mn–S4	78.8(3)	∠O2–Ge3–S7	110.3(3)
∠S8–Mn–S4	107.10(14)	∠S2–Ge3–S7	113.29(14)
∠S3–Mn–S4	171.78(14)	∠S5–Ge3–S7	114.65(14)

4 References

[1] P. Kubelka, An article on optics of paint layers, *Z. Tech. Phys.*, 1931, **12**, 593–601.

[2] CrystalClear Version 1.3.5; Rigaku Corp.: Woodlands, TX, 1999.

[3] G. M. Sheldrick, A short history of SHELX, *Acta Crystallogr., Sect. A: Found. Crystallogr.* 2008, 112–122.

[4] G. Kresse, VASP, 5.3.5; http://cms.mpi.univie.ac.at/vasp/vasp/vasp.html.

[5] G. Kresse and J. Furthmuller, Efficient iterative schemes for ab initio total-energy calculations using a plane-wave basis set. *Phys. Rev. B: Condens. Matter,* 1996, **54**, 11169–11186.

[6] G. Kresse and D. Joubert, From ultrasoft pseudopotentials to the projector augmented-wave method. *Phys. Rev. B: Condens. Matter,* 1999, **59**, 1758–1775.

[7] P. E. Blochl, Projector augmented-wave method. *Phys. Rev. B: Condens. Matter ,*1994, **54**, 17953–17979.

[8] J. P. Perdew, K. Burke and M. Ernzerhof, Generalized Gradient Approximation Made Simple. *Phys. Rev. Lett.,* 1996, **77**, 3865–3868.

[9] D. J. Chadi, Special points for Brillouin-zone integrations. *Phys. Rev. B: Condens. Matter,* 1976, **16**, 1746–1747.